Electronic Supplementary Material (ESI) for Dalton Transactions.

Supporting Information

Biomimetic Catalysts of Iron-based Metal-Organic Frameworks with High Peroxidase-Mimicking Activity for Colorimetric Biosensing

Xiaoning Wang[a], Yumeng Zhao[b], Jialuo Li[c], Jiandong Pang[c], Qiang Wang[a], Bao Li[*b] and Hong-Cai Zhou[*c]

[a] Hubei Key Laboratory of Biomass Fibers and Eco-dyeing & Finishing, *College of Chemistry and Chemical Engineering, Wuhan Textile University, Wuhan, Hubei, 430073, PR China.*

[b] *Key Laboratory of Material Chemistry for Energy Conversion and Storage, School of Chemistry and Chemical Engineering, Huazhong University of Science and Technology, Wuhan, Hubei, 430074, PR China.*

[c] *Department of Chemistry, Texas A&M University, College Station, Texas 77843-3255, United States.*

*E-mails: libao@hust.edu.cn; zhou@chem.tamu.edu

Content

S1. Materials and General Methods

The organic ligand H_6L and other reagents for the syntheses were of analytical grade and used as received from commercial sources without further purification. Elemental analyses for C, H, and N were performed on a Perkin-Elmer 2400 elemental analyzer. The IR spectra were recorded with KBr pellets on a Nicolet Avatar-360 spectrometer in the 4000–400 cm^{-1} region. Powder X-ray diffraction (PXRD) was carried out on a Bruker D8-Focus Bragg-Brentano X-ray Powder Diffractometer equipped with a Cu sealed tube (λ = 1.54178 Å) at 40 kV and 40 mA. Thermogravimetry analysis (TGA) was conducted on a TGA-50 thermogravimetric analyzer. Diffraction was measured on a Bruker Venture CMOS diffractometer equipped with a Cu-*K*α sealed-tube X-ray source (λ = 1.54178 Å) at 100 K. The N_2 sorption measurements were conducted using a Micrometritics ASAP 2020 system. Ultraviolet-visible (UV-vis) adsorption spectra of the samples were recorded on UV-3600 spectrophotometer.

S2. Syntheses

S2.1 Synthesis of HUST-5. The crystal sample HUST-5 was synthesized according to our previous work with little modification as follows[1]: $FeCl_2 \cdot 4H_2O$ (0.18 mmol, 36 mg) and H_6L (0.042 mmol, 40 mg) were ultrasonically dissolved in 12 mL DMF and 1 mL H_2O, and formic acid (1.6 mL) was then added to the solution in a 20 mL glass vial. The vial was then heated at 120 °C for 5 days in an oven. After cooling to room temperature, the red block crystals were harvested by filtration and washed with DMF. The yield was 48% for HUST-5 (based on H_6L ligand). IR (KBr, cm^{-1}): 3422 (m, br), 3072 (w), 2928 (w), 1658 (m), 1598 (vs), 1549 (m), 1410 (vs), 1266 (m), 1206 (s), 1153 (vs), 1018 (w), 950 (s), 887 (m), 788 (s), 697 (m), 617 (m), 478 (m).

Elemental analysis calcd (%) for HUST-5 ($C_{85}H_{57}Fe_6N_6O_{44}P_6$): C 42.76, H 2.41, N 3.52; Found: C 43.40, H 2.85, N 4.06.

S2.2 Synthesis of HUST-7. $FeCl_2 \cdot 4H_2O$ (0.18 mmol, 36 mg) and H_6L (0.042 mmol, 40 mg) were ultrasonically dissolved in 12 mL DMF and 1 mL H_2O, and acetic acid (1.6 mL) was then added to the solution in a 20 mL glass vial. The vial was then heated at 120 °C for 5 days in an oven. After cooling to room temperature, the red plate shaped crystals were harvested by filtration and washed with DMF. The yield was 43% for HUST-7 (based on H_6L ligand). IR (KBr, cm^{-1}): 3425 (m, br), 3077 (w), 2926 (w), 1670 (s), 1607 (s), 1564 (m), 1409 (vs), 1272 (m), 1200 (s), 1158 (vs), 1099 (m), 1012 (m), 940 (s), 889 (m), 783 (m), 734 (m), 697 (m), 619 (m), 469 (m). Elemental analysis calcd (%) for HUST-7 ($C_{42}H_{28}Fe_3N_3O_{22}P_3$): C 42.49, H 2.37, N 3.54; Found: C 43.28, H 2.97, N 4.10.

S3. X-Ray Structural Determination

Diffraction data for HUST-7 has been collected via Bruker Venture using Cu-*Kα* (λ = 1.54178 Å) radiation at 100 K. The structures of complexes were solved by direct methods, and the non-hydrogen atoms were located from the trial structure and then refined anisotropically with SHELXTL using a full-matrix leastsquares procedure based on F^2 values. The hydrogen atom positions were fixed geometrically at calculated distances and allowed to ride on the parent atoms. Attempts to define the highly disordered solvent molecules were unsuccessful, so the structure was refined with the PLATON "SQUEEZE" procedure. After the calculation of TGA and SQUEEZE, the whole formula of HUST-7 should be $C_{42}H_{30}Fe_3N_3O_{22}P_3 \cdot 4H_2O \cdot 5C_3H_7NO$. The diffraction intensity of crystal sample was very weak due to the very small size and large porous framework, which must be

responsible for the corresponding alert A. CCDC-1913173, 1954084 for the data under different temperature contain the supplementary crystallographic data for this paper. The data can be obtained free of charge from The Cambridge Crystallographic Data Centre via http://www.ccdc.cam.ac.uk/data_request/cif (or from the Cambridge Crystallographic Data Centre, 12 Union Road, Cambridge CB2 1EZ, U.K.). The details for structural analyses of the HUST-5 and HUST-7 were listed in Table S1-3.

S4. N_2 Sorption Measurements

Before gas sorption experiments, as-synthesized HUST-7 samples were washed with DMF and immersed in acetonitrile for 3 days, during which the solvent was decanted and freshly replenished three times. The solvent was removed under vacuum at 80 ℃, yielding porous material. Gas sorption measurements were then conducted using a Micrometritics ASAP 2020 system.

S5. Computational Detail

Spin polarized DFT calculations were performed by using DMol^3 software in the Material Studio module.[2] Exchange-correlation (XC) effects were described by Perdew–Burke–Ernzerhof (PBE) functional with generalized gradient approximation (GGA).[3] All electron numerical basis set of double numerical plus polarization (DNP),[4] comparable to the 6-31G** Gaussian basis sets and featuring less basis set superposition error (BSSE),[5] were used to expand electronic wave function. For Fe, the Effective Core Potentials (ECP)[6] replaces core electrons by a single effective potential, and valence electrons were described by DNP numerical basic set. DFT-D corrections with Grimme method[7] was used to the treatment of weak dispersion energy. In the optimization calculation, 1.0×10^{-5} Ha and 1.0×10^{-3} Ha. Å^{-1} were set as the convergence value of energy and force, and the threshold for SCF density convergence was 1.0×10^{-6}. Adsorption energy were typically calculated based following formula: $E_a(X) = E(X\text{-}MOF) - E(MOF) - E(X)$(X= OPD, THB and TMB), where E(X- MOF), E(MOF) and E(X) were single-point energy of relaxed

geometry of X-MOF, MOF and three reaction species with the same computational setting. Meanwhile, dissociation energy of aqua ligand was evaluated according to this formula: E_d = E(H_2O) + E(MOF-H_2O) – E(MOF), where E(MOF), E(MOF-H_2O) and E(H_2O) were single-point energy of relaxed structure of original MOF, H_2O-removed MOF and H_2O with the same computational setting.

S6. Crystal Data

Table S1. Crystal Data of HUST-7

	HUST-7
Empirical formula	$C_{57}Fe_3H_{73}N_8O_{31}P_3$
Formula weight	1626.707
Temperature/K	100.00
Crystal system	orthorhombic
Space group	*P*bam
a/Å	22.234(4)
b/Å	28.096(6)
c/Å	28.408(6)
α/°	90
β/°	90
γ/°	90
Volume/Å^3	17746(6)
Z	8
ρ_{calc}g/cm^3	1.218
μ/mm^{-1}	0.611
F(000)	6751.2
Crystal size/mm^3	0.2 × 0.2 × 0.15
Radiation	Mo Kα (λ = 0.71073)
2Θ range for data collection/°	2.74 to 44.52

Index ranges	$0 \le h \le 23, 0 \le k \le 29, 0 \le l \le 29$
Reflections collected	11074
Data/restraints/parameters	11074/0/680
Goodness-of-fit on F^2	1.055
Final R indexes [I>=2σ (I)]	$R_1 = 0.0648$, $wR_2 = 0.1903$
Final R indexes [all data]	$R_1 = 0.0684$, $wR_2 = 0.1961$
Largest diff. peak/hole / e $Å^{-3}$	0.55/-0.47

Table S2 Selected Bond Lengths for HUST-5

Atom	**Atom**	**Length/Å**	**Atom**	**Atom**	**Length/Å**
Fe1	O2	2.060(9)	O28	Fe5[3]	1.990(9)
Fe1	O41	1.969(10)	O26	Fe6[3]	2.025(9)
Fe1	O24	1.971(9)	C60	C59	1.439(11)
Fe1	O4	1.965(10)	O42	Fe6	2.080(13)
Fe1	O38	1.978(9)	O30	Fe6[4]	1.936(10)
Fe1	O7[1]	2.040(11)	O12	Fe6[2]	1.977(9)
O11	Fe4[2]	2.030(8)	O23	Fe3	1.984(9)
O8	Fe2[2]	1.976(10)	O3	Fe3	1.934(10)
O44	Fe5	1.891(11)	O9	Fe3[2]	2.037(9)
O44	Fe4	1.919(9)	O6	Fe3[5]	2.010(11)
O44	Fe6	1.935(9)	Fe2	O8[1]	1.976(10)
O41	Fe2	1.944(10)	Fe2	O10[1]	1.968(10)

O41	Fe3	1.849(10)	Fe2	O5[5]	2.036(10)
O10	Fe2[2]	1.968(10)	Fe3	O9[1]	2.037(9)
O27	Fe4[3]	1.991(8)	Fe3	O6[5]	2.010(11)
O22	Fe5	2.008(10)	Fe5	O29[6]	2.043(10)
O19	Fe4	2.008(10)	Fe5	O28[7]	1.990(9)
O1	Fe2	1.960(9)	Fe4	O11[1]	2.030(8)
O29	Fe5[4]	2.043(10)	Fe4	O27[7]	1.991(8)
O25	Fe4[3]	2.051(12)	Fe4	O25[7]	2.051(12)
O43	Fe5	2.061(10)	Fe6	O26[7]	2.025(9)
O5	Fe2[5]	2.036(10)	Fe6	O30[6]	1.936(10)
O21	Fe6	2.082(9)	Fe6	O12[1]	1.977(9)
O40	Fe3	2.066(12)	O7	Fe1[2]	2.040(11)
O20	Fe5	1.945(10)			

[1]-1/2+X,1/2+Y,+Z; [2]1/2+X,-1/2+Y,+Z; [3]-1/2+X,-1/2+Y,+Z; [4]5/2-X,-1/2+Y,-Z; [5]3-X,+Y,-1-Z; [6]5/2-X,1/2+Y,-Z; [7]1/2+X,1/2+Y,+Z

Table S3. Selected Bond Lengths for HUST-7

Atom	Atom	Length/Å	Atom	Atom	Length/Å
Fe1	O8[1]	2.124(4)	Fe4	O23	1.896(4)
Fe1	O8	2.124(4)	Fe4	O26	2.059(6)
Fe1	O12[2]	2.108(4)	Fe5	O13[6]	2.023(4)
Fe1	O12[3]	2.108(4)	Fe5	O13	2.023(4)
Fe1	O19	1.999(5)	Fe5	O16[8]	2.017(4)

Fe1	O22	2.067(8)	Fe5	O16[9]	2.017(4)
Fe2	O7[1]	1.981(5)	Fe5	O23	1.928(5)
Fe2	O7	1.981(5)	Fe5	O24	2.050(6)
Fe2	O9[4]	2.032(4)	Fe6	O15[8]	2.029(4)
Fe2	O9[5]	2.032(4)	Fe6	O15[9]	2.029(4)
Fe2	O19	1.852(4)	Fe6	O18[7]	2.007(4)
Fe2	O20	2.141(6)	Fe6	O18[4]	2.007(4)
Fe3	O10[4]	2.044(4)	Fe6	O23	1.937(5)
Fe3	O10[5]	2.044(4)	Fe6	O25	2.044(7)
Fe3	O11[2]	2.005(4)	O9	Fe2[5]	2.032(4)
Fe3	O11[3]	2.005(4)	O10	Fe3[5]	2.044(4)
Fe3	O19	1.897(5)	O11	Fe3[10]	2.005(4)
Fe3	O21	2.077(6)	O12	Fe1[10]	2.109(4)
Fe4	O14	2.013(4)	O15	Fe6[11]	2.029(4)
Fe4	O14[6]	2.013(4)	O16	Fe5[11]	2.017(4)
Fe4	O17[7]	2.006(5)	O17	Fe4[7]	2.006(5)
Fe4	O17[4]	2.006(5)	O18	Fe6[7]	2.006(4)

[1]+X,+Y,-Z; [2]1/2-X,1/2+Y,+Z; [3]1/2-X,1/2+Y,-Z; [4]1-X,1-Y,+Z; [5]1-X,1-Y,-Z; [6]+X,+Y,1-Z; [7]1-X,1-Y,1-Z; [8]1/2+X,1/2-Y,1-Z; [9]1/2+X,1/2-Y,+Z; [10]1/2-X,-1/2+Y,-Z; [11]-1/2+X,1/2-Y,+Z

S7. The Crystal Images of HUST-5 and HUST-7

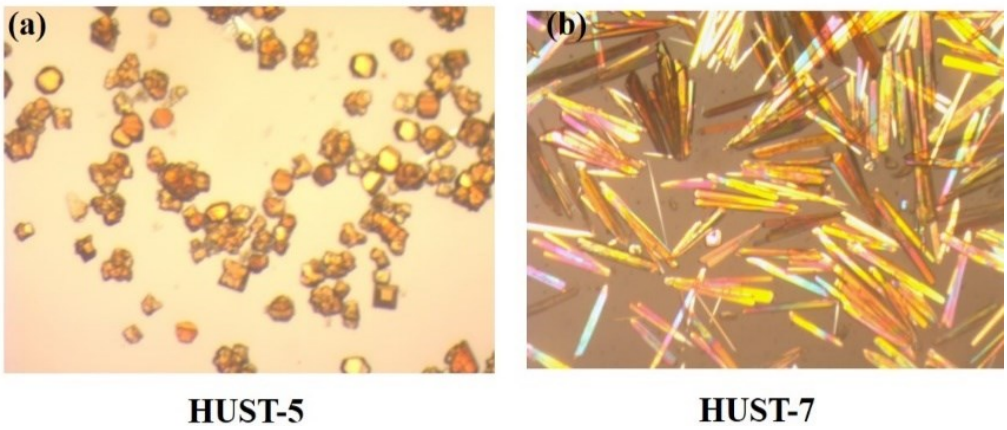

Figure S1. Optical microscopic photographs of HUST-5 (a) and HUST-7 (b).

S8. The Crystal Structure of HUST-5 and HUST-7

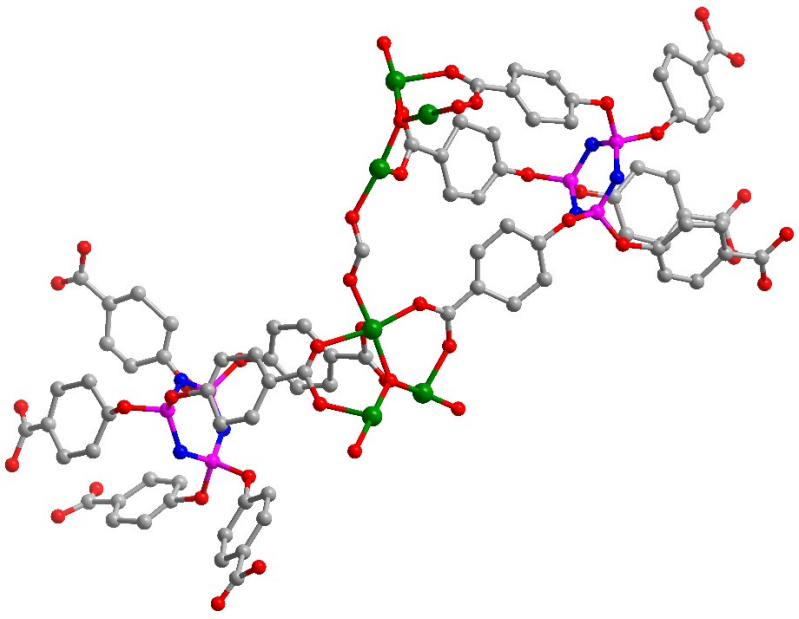

(a)

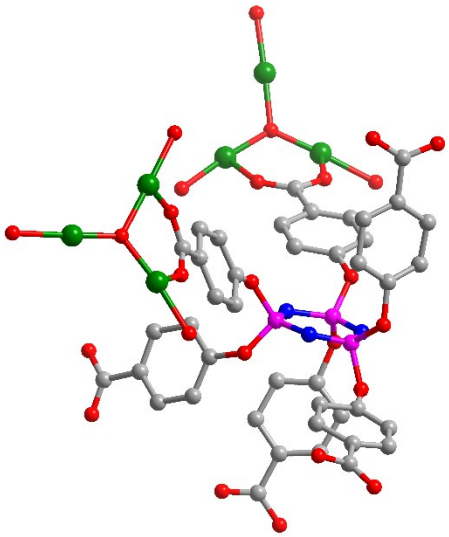

(b)

Figure S2. The asymmetric unit of HUST-5 and HUST-7.

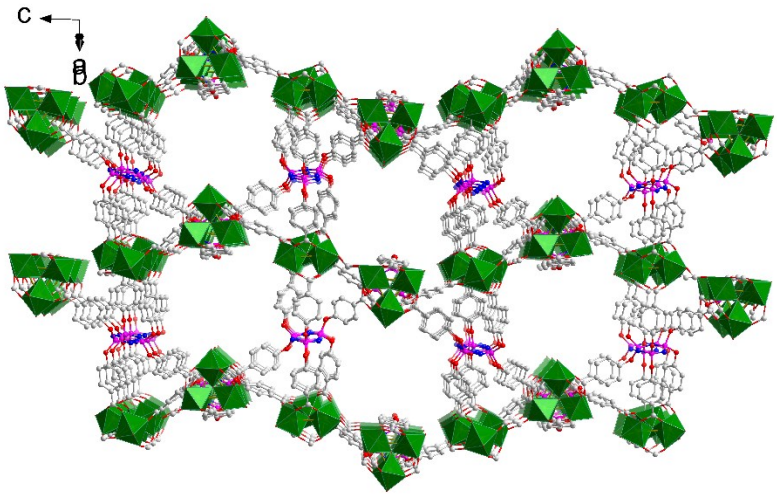

Figure S3. Partial view of two-dimensional channels of HUST-5.

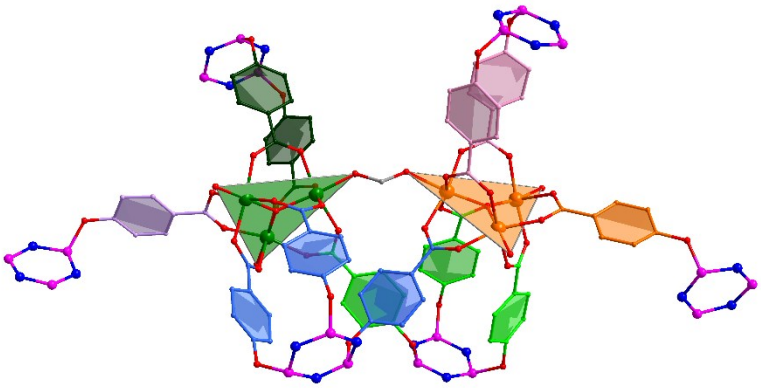

Figure S4. The coordination environment of hexa-nuclear clusters in HUST-5.

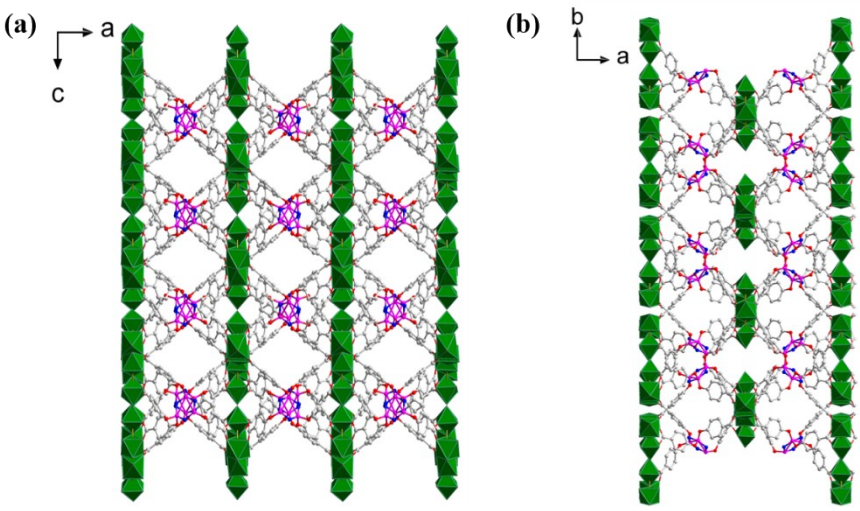

Figure S5. Partial view of 3D structure of HUST-7 along b axis (a) and c axis (b).

S9. TGA Curves of HUST-5 and HUST-7

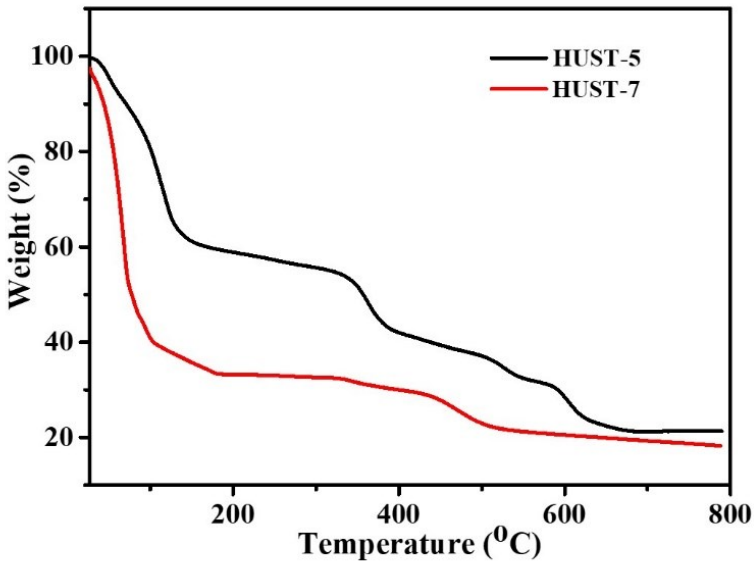

Figure S6. TGA curves of the as-prepared HUST-5 and HUST-7.

S10. Powder X-ray Diffraction

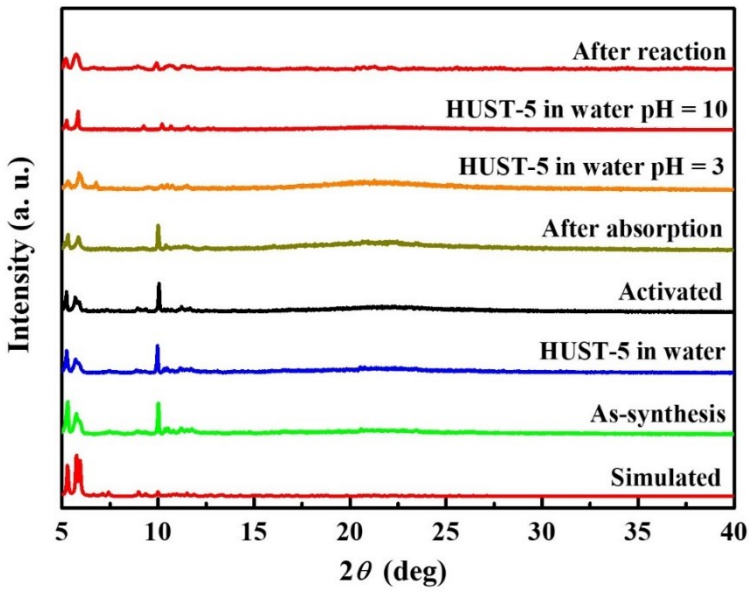

Figure S7. PXRD patterns of the simulated HUST-5 and as-synthesized HUST-5 under different conditions.

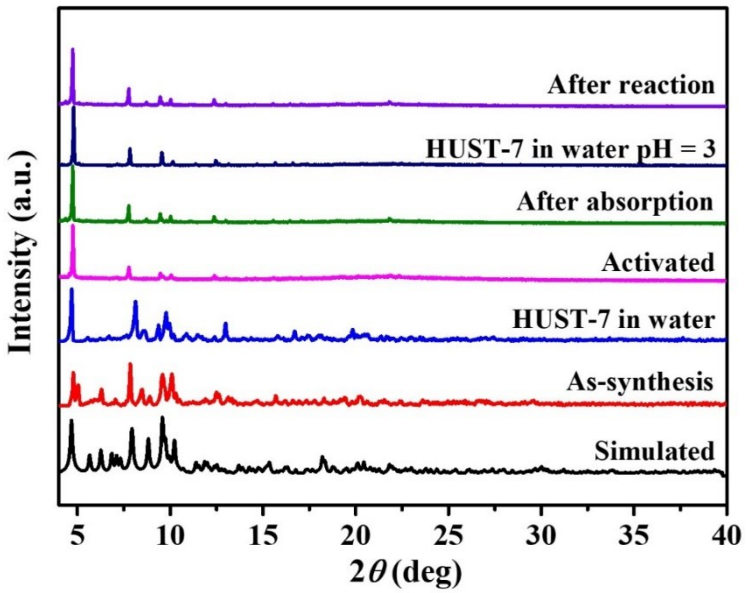

Figure S8. PXRD patterns of the simulated HUST-7 and as-synthesized HUST-7 under different conditions.

S11. Catalytic Activity Test and H_2O_2 and AA Detection Procedures

To examine the peroxidase-like activity, the catalytic oxidation of the peroxidase substrates in the presence of H_2O_2 was conducted by Fe-MOFs, HUST-5 and HUST-7. The products were confirmed by scanning the UV-vis absorbance on spectrophotometer and the concentrations of products were calculated by their molar extinction coefficients at respective wavelengths (for oxTMB is 35800 $M^{-1}\cdot cm^{-1}$ at 661 nm; for oxOPD is 16300$\cdot M^{-1}$ cm^{-1} at 450 nm). For kinetic study of the single substrate reaction, we propose the reactions catalyzed by Fe-MOFs follow widely-accepted ping-pong mechanism. Lineweaver–Burk plot was employed for illustrating kinetic data and calculate the parameters by taking the reciprocal of both sides of the Michaelis–Menten equation.

$$\frac{1}{v} = \frac{K_m}{v_{max}[S]} + \frac{1}{v_{max}}$$

in which v and v_{max} are the initial reaction rate and the maximal reaction rate, respectively. [S] is the concentration of the substrate and K_m is the Michaelis-Menten constant.

Typical TMB Oxidation Procedure Catalyzed by Fe-MOFs

In a typical assay, 80 μL of Fe-MOFs dispersion (1 mg mL^{-1}) were mixed in 1600 μL of NaAc buffer solution (pH = 4.0), followed by adding 400 μL of TMB solution (1 mM, ethanol solution). Then, 40 μL of H_2O_2 solution (4.2 mM) was added into the mixture. The mixed solution was incubated at 45 °C for 10 min for standard curve measurement.

Kinetic Measurements

Kinetic measurements were carried out in time course mode by monitoring the

absorbance change at 660 nm or 450 nm. To investigate the mechanism, assays were carried out by varying concentrations of TMB or OPD at a fixed concentration of H_2O_2 or vice versa.

For oxidation of TMB, NaAc buffer solution (pH = 4.0) was selected due to the favorable reaction condition. The concentrations of substrate varied from 0.3 mM to 1.8 mM along with a fixed amount of HUST-5 catalyst (0.038 mg mL^{-1}) and hydrogen peroxide concentration of 99.7 mM. The reaction was carried out at 45 °C for 6 min and the content of oxTMB was assessed through the UV absorbance.

For oxidation of OPD, NaAc buffer solution (pH = 4.0) was selected due to the favorable reaction condition. The concentrations of substrate varied from 0.67 mM to 2.4 mM along with a fixed amount of HUST-5 catalyst (0.038 mg mL^{-1}) and hydrogen peroxide concentration of 266 mM. The reaction was carried out at 45 °C for 6 min and the content of oxOPD was assessed through the UV absorbance.

Detection of H_2O_2 using Fe-MOFs as peroxidase mimetics

To investigate the peroxidase-like activity of the as-prepared Fe-MOFs, the catalytic oxidation of the peroxidase substrate TMB in the presence of H_2O_2 was tested. The measurements were carried out by monitoring the absorbance change of oxTMB at 661 nm. In a typical experiment process, 80 μL of Fe-MOFs dispersion (1 mg mL^{-1}) were mixed in 1600 μL of NaAc buffer solution (pH = 4.0), followed by adding 400 μL of TMB solution (1 mM, ethanol solution). Then, 10 μL of H_2O_2 of various concentrations was added into the mixture. The mixed solution was incubated at 40 °C for 10 min for standard curve measurement.

Detection of ascorbic acid using Fe-MOFs by inhibiting the TMB oxidation

Ascorbic acid detection was carried out as follows: 400 μL of TMB solution (1 mM, ethanol solution) and 20 μL AA of various concentrations was added into 1600 μL of NaAc buffer solution (pH = 4.0), followed by adding 80 μL of Fe-MOFs dispersion (1

mg mL^{-1}). Then, 10 μL of H_2O_2 (30 wt%) was added into the mixture. The mixture was incubated at 40 °C for 10 min. Then UV-Vis spectra measurements and photographs were taken.

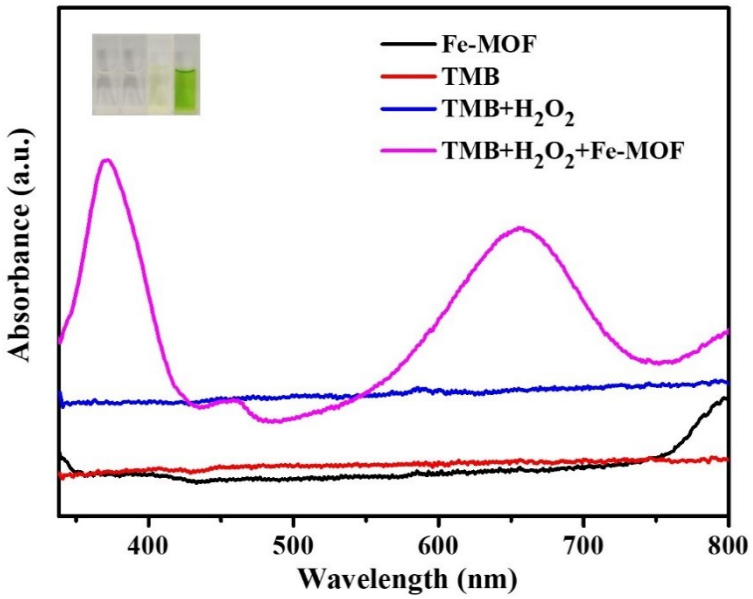

Figure S9. UV-vis adsorption spectra for TMB, TMB-H_2O_2, TMB-H_2O_2-Fe-MOF and Fe-MOF solutions in pH = 4.0 NaAc buffer solution.

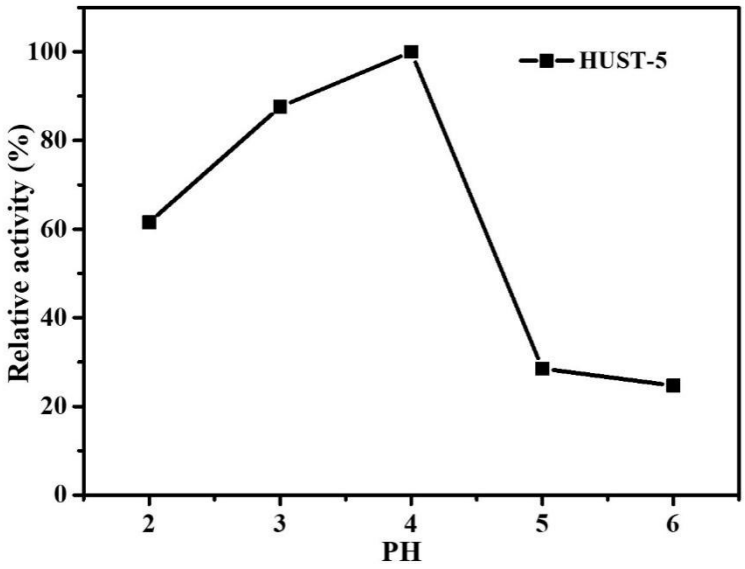

(a)

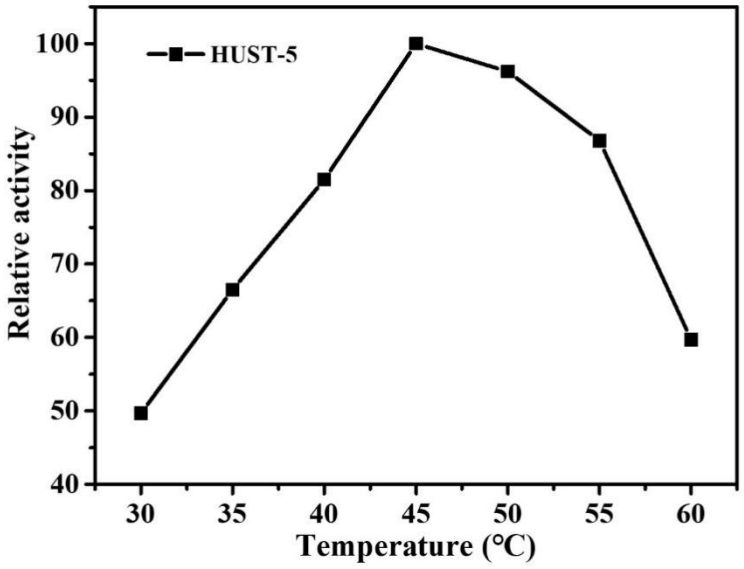

(b)

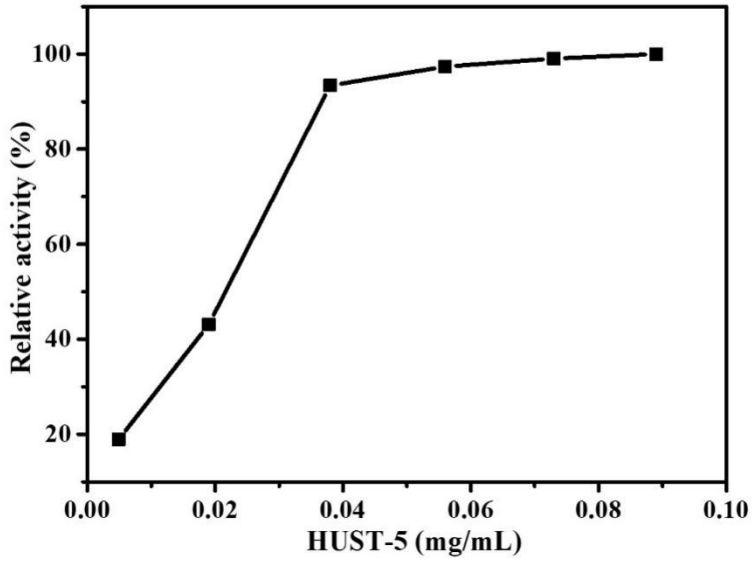

(c)

Figure S10. Peroxidase-like catalytic activity of HUST-5 against (a) pH value, (b) temperature, and (c) catalyst dosage. The maximum activity in each graph was set as 100%.

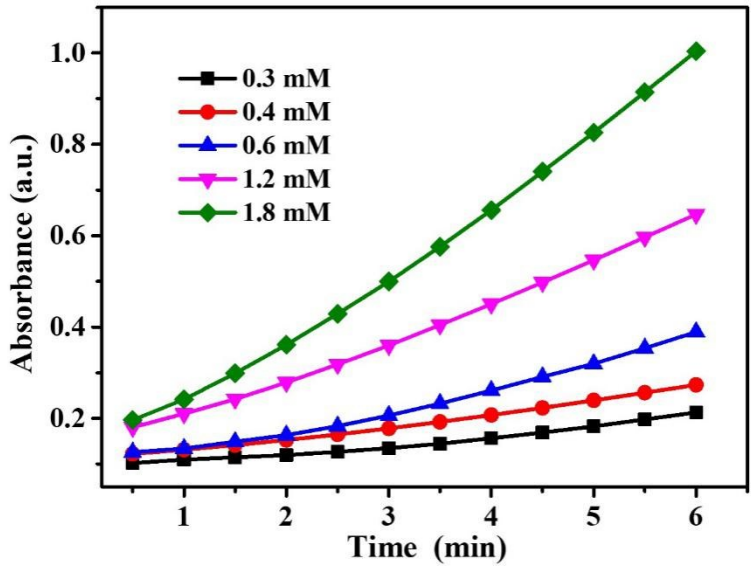

Figure S11. The time-dependent absorbance changes at 660 nm of various concentrations of TMB catalyzed by HUST-5.

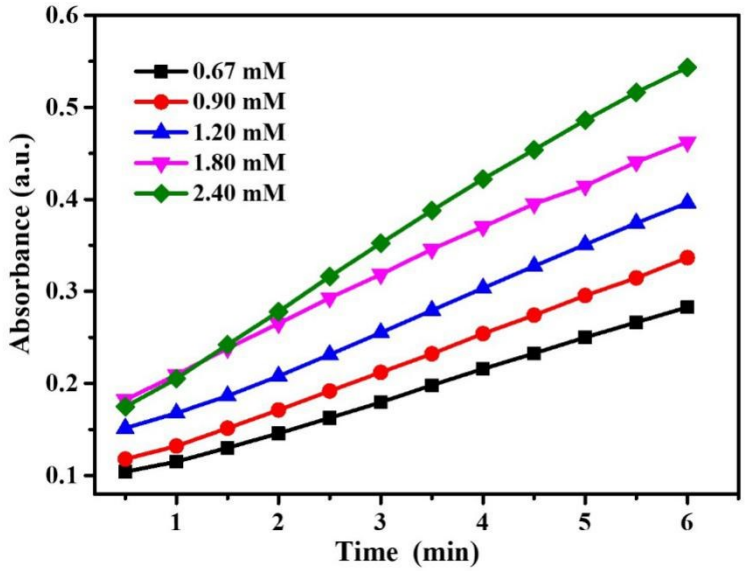

Figure S12. The time-dependent absorbance changes at 450 nm of various concentrations of OPD catalyzed by HUST-5.

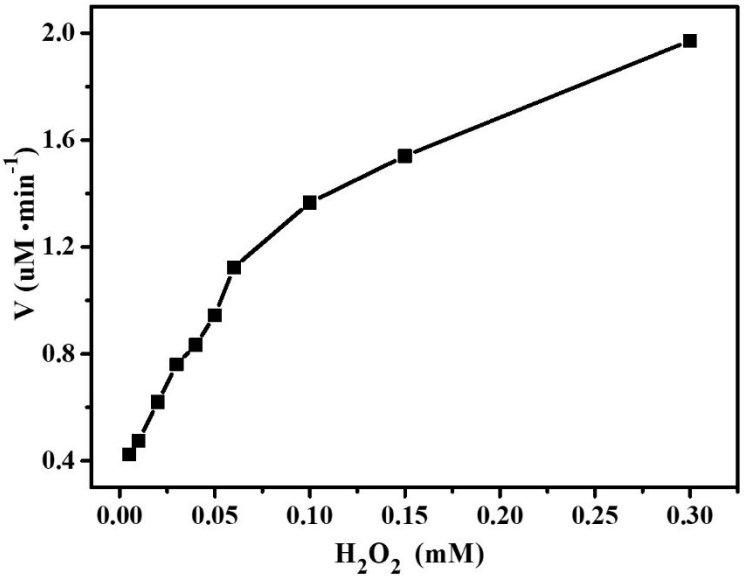

(a)

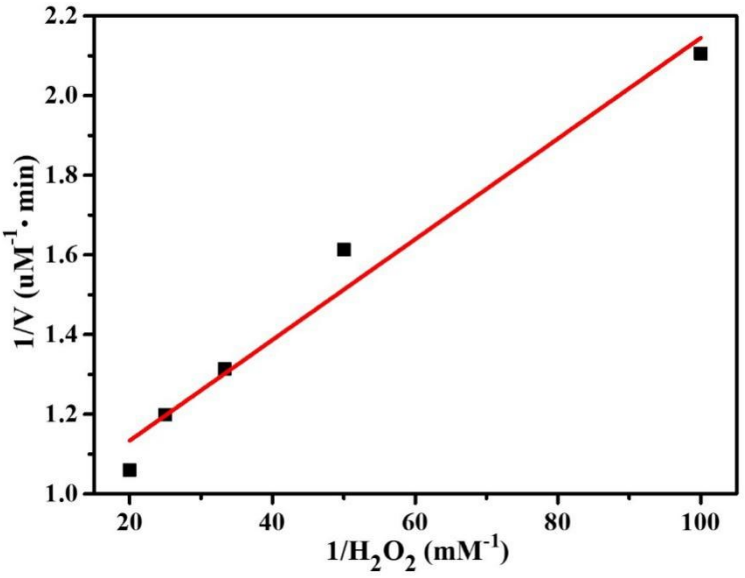

(b)

Figure S13. The velocity of the TMB oxidation reaction catalyzed by HUST-5. The concentrations of H_2O_2 range from 5 to 300 μM. (b) Double-reciprocal plots of the activity of HUST-5 at a fixed TMB concentration with different concentration of the second substrate H_2O_2.

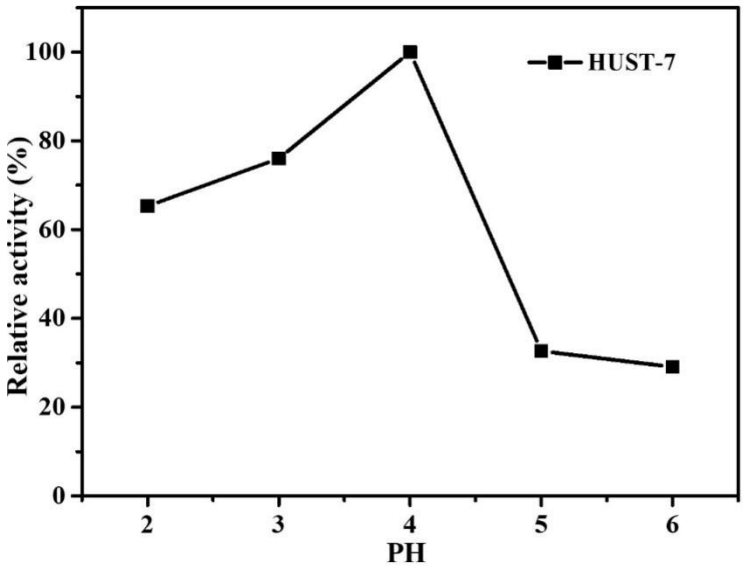
HUST-7
Relative activity (%)
100
80
60
40
20
0
2
3
4
5
6
PH

(a)

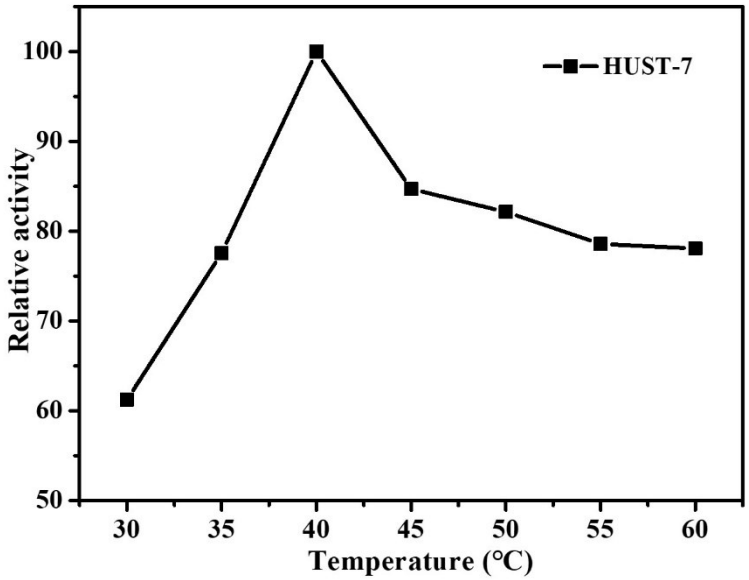
HUST-7
Relative activity
100
90
80
70
60
50
30
35
40
45
50
55
60
Temperature (°C)

(b)

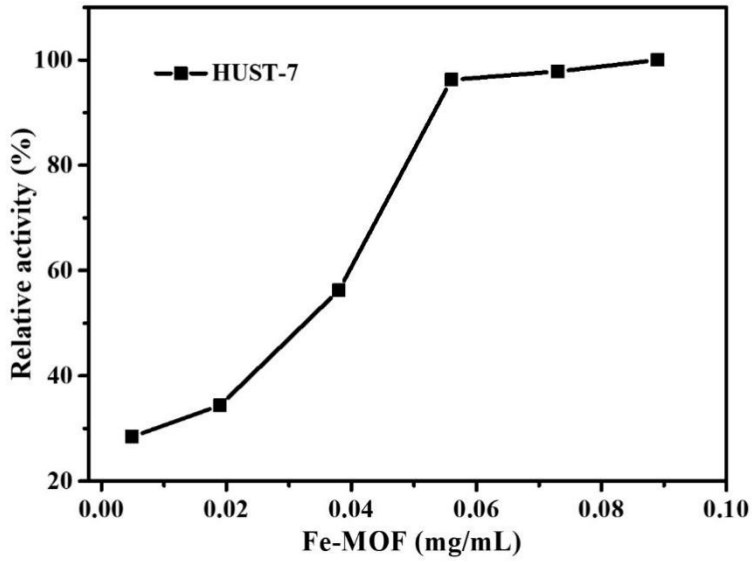

(c)

Figure S14. The Peroxidase-like catalytic activity of HUST-7 against (a) pH value, (b) temperature, and (c) catalyst dosage. The maximum activity in each graph was set as 100%.

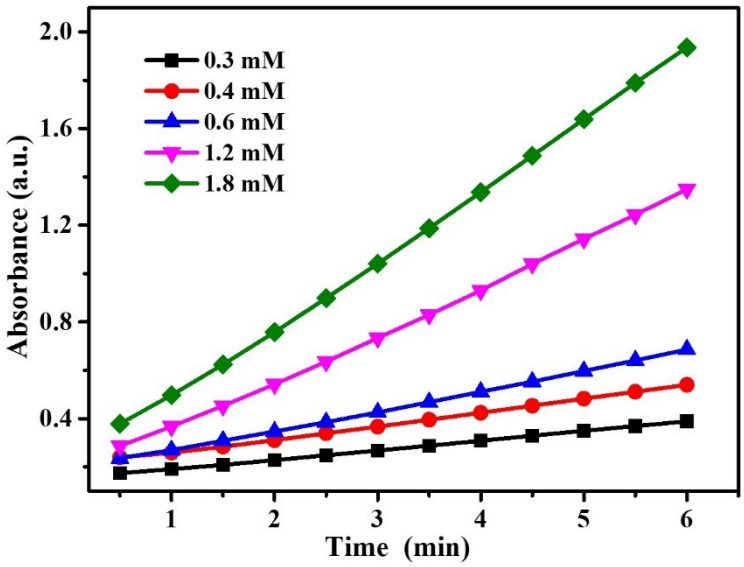

Figure S15. The time-dependent absorbance changes at 660 nm of various concentrations of TMB catalyzed by HUST-7.

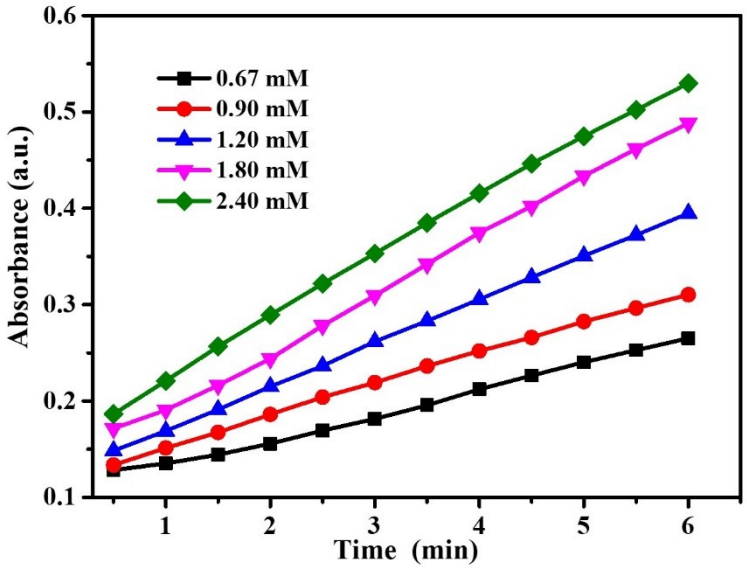

Figure S16. The time-dependent absorbance changes at 450 nm of various concentrations of OPD catalyzed by HUST-7.

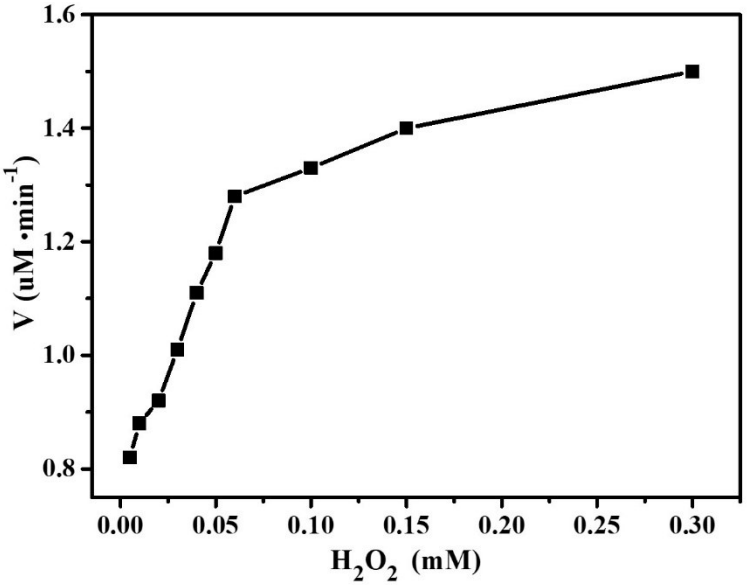

(a)

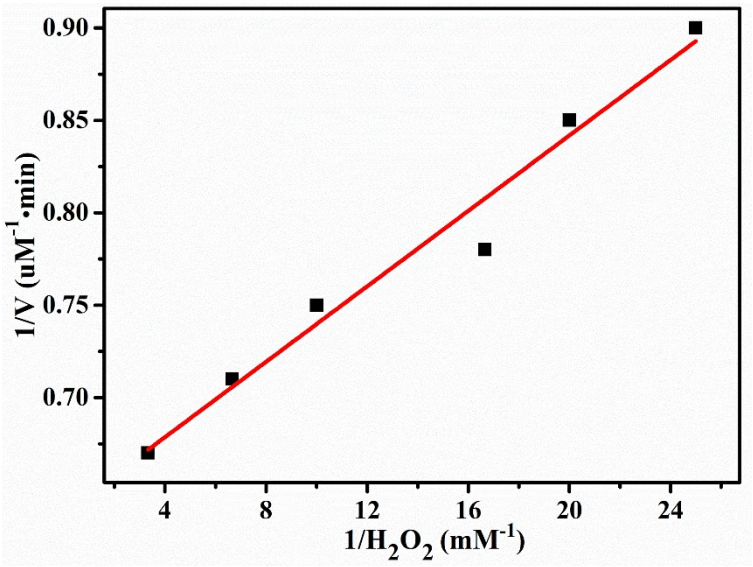

(b)

Figure S17. The velocity of the TMB oxidation reaction catalyzed by HUST-7. The concentrations of H_2O_2 range from 5 to 300 μM. (b) Double-reciprocal plots of the activity of HUST-7 at a fixed TMB concentration with different concentration of the second substrate H_2O_2.

Table S4. Apparent Michaelis−Menten constant (K_m) and maximum reaction rate (V_{max}) of Fe-MOFs and other materials.

Catalyst	Substrate fixed	Substrate varied	K_m [mM]	V_{max} [M s^{-1}]	Ref
HUST-5	TMB	H_2O_2	0.014	1.89×10^{-8}	**This work**
	H_2O_2	TMB	3.57	2.12×10^{-7}	
HUST-7	TMB	H_2O_2	0.016	1.57×10^{-8}	**This work**
	H_2O_2	TMB	4.9	5.27×10^{-7}	
MIL-53(Fe)	TMB	H_2O_2	0.04	1.86×10^{-8}	8

	H_2O_2	TMB	1.08	8.78×10^{-8}	
	TMB	H_2O_2	1.06	1.39×10^{-8}	
MOF-808					9
	H_2O_2	TMB	0.0796	3.12×10^{-8}	
	TMB	H_2O_2	3.7	8.71×10^{-8}	
HRP					10
	H_2O_2	TMB	0.434	1.00×10^{-7}	
	TMB	H_2O_2	0.10	1.40×10^{-7}	
N-GODs					11
	H_2O_2	TMB	11.19	3.80×10^{-7}	
	TMB	H_2O_2	3.9	3.85×10^{-8}	
GO-COOH					12
	H_2O_2	TMB	0.024	3.45×10^{-8}	
	TMB	H_2O_2	10.9	8.98×10^{-8}	
H@M					13
	H_2O_2	TMB	0.068	6.07×10^{-8}	
	TMB	H_2O_2	154	9.78×10^{-8}	
Fe_3O_4 MNPs					14
	H_2O_2	TMB	0.098	3.44×10^{-8}	

Table S5. Comparison of the sensing parameters among MOF-Based peroxidase mimics for their colorimetric sensing of H_2O_2 and AA.

Peroxidase mimic	Analyte	Linear range (μM)	Detection limit (μM)	Ref
HUST-5	H_2O_2	5-50	1.84	**This work**
HUST-7	H_2O_2	5-50	4.26	**This work**
MIL-53(Fe)	H_2O_2	0.95−19	0.13	8
MOF-808	H_2O_2	10−15000	4.5	9

$Cu_6(Trz)_{10}(H_2O)_4[H_2SiW_{12}O_{40}]$	H_2O_2	10−50	1.37	15
MIL-68(Fe)	H_2O_2	3-40	0.256	16
MIL-100(Fe)	H_2O_2	3-40	0.155	16
HUST-5	AA	37.91-341.23	12.11	**This work**
HUST-6	AA	37.91-341.23	15.92	**This work**
MIL-53(Fe)	AA	28.6−190.5	15	8
MOF-808	AA	30−1030	15	9
MIL-68(Fe)	AA	30−485	6	16
MIL-100(Fe)	AA	30−485	6	16

References

[1] F. Yu, B. Q Hu, X. Wang, Y. Zhao, J. Li, B. Li and H. Zhou, *J. Mater. Chem. A,* 2020, **8**, 2083-2089.

[2] (a) B. Delley, *J. Chem. Phys*., 1990, **92**, 508-517; (b) B. Delley, *J. Chem. Phys*., 1991, **94**, 7245-7250; (c) B. Delley, *J. Chem. Phys.,* 2000, **113**, 7756-7764.

[3] H. J. Monkhorst and J. D. Pack, *Phys. Rev. B,* 1976, **13**, 5188-5192.

[4] J. P. Perdew, K. Burke and M. Ernzerhof, *Phys. Rev. Lett.,* 1996, **77**, 3865-3868.

[5] Y. Inada and H. orita, *J. Comput. Chem.,* 2008, **29**, 225-232.

[6] M. Dolg, U. Wedig, H. Stoll and H. Preuss, *J. Chem. Phys*., 1987, **86**, 866-872.

[7] S. Grimme, *J. Comput. Chem.,* 2006, **27**, 1787-1799.

[8] L. Ai, L. Li, C. Zhang, J. Fu and J. Jiang, *Chem. -Eur. J.,* 2013, **19**, 15105-15108.

[9] H. Zheng, C. Liu, X. Zeng, J. Chen, J. Lü, R. Lin, R. Cao, Z. Lin and J. Su, *Inorg. Chem.,* 2018, **57**, 9096-9104.

[10] M. Liu, H. Zhao, S. Chen, H. Yu and X. Quan, *ACS Nano.,* 2012, **6**, 3142-3151.

[11] L. Lin, X. Song, Y. Chen, M. Rong, T. Zhao, Y. Wang, Y. Jiang and X. Chen, *Anal. Chim. Acta.,* 2015, **869**, 89-95.

[12] Y. Song, K. Qu, C. Zhao, J. Ren and X. Qu, *Adv. Mater.,* 2010, **22**, 2206-2210.

[13] F. Qin, S. Jia, F. Wang, S. Wu, J. Song and Y. Liu, *Catal. Sci. Technol.,* 2013, **3**, 2761-2768.

[14] L. Su, J. Feng, X. Zhou, C. Ren, H. Li and X. Chen, *Anal. Chem.,* 2012, **84**, 5753-5758.

[15] E. Zhou, C. Qin, P. Huang, X. Wang, W. Chen, K. Shao and Z. Su, *Chem. -Eur. J.,* 2015, **21**, 11894-11898.

[16] J. Zhang, H. Zhang, Z. Du, X. Wang, S. Yu and H. Jiang, *Chem. Commun.,* 2014, **50**, 1092-1094.